General Disclaimer

One or more of the Following Statements may affect this Document

- This document has been reproduced from the best copy furnished by the organizational source. It is being released in the interest of making available as much information as possible.

- This document may contain data, which exceeds the sheet parameters. It was furnished in this condition by the organizational source and is the best copy available.

- This document may contain tone-on-tone or color graphs, charts and/or pictures, which have been reproduced in black and white.

- This document is paginated as submitted by the original source.

- Portions of this document are not fully legible due to the historical nature of some of the material. However, it is the best reproduction available from the original submission.

Semiannual Status Report

to

National Aeronautics and Space Administration

from

The University of Texas at Dallas
P. O. Box 688
Richardson, Texas 75080
(214) 690-2111

Grant NGL 44-004-026

For the Period Ending 15 March 1975

F. S. Johnson

Principal Investigator

June 1975

Transport Processes in the Upper Atmosphere

F. S. Johnson

Work in this area has concentrated on two problems: energetics of turbulence in stable atmospheres, and the atomic oxygen minimum in the vicinity of the equator.

There is some evidence, mostly from boundary layers, that turbulence sometimes remains constant in a stable atmosphere with Richardson numbers in the vicinity of 0.25, or perhaps in the range 0.25 - 0.50. Since the Richardson number is the ratio of the rate of doing work against buoyancy forces to the rate of extraction of energy from shear, such observations imply that 1 to 3 times as much energy is expended against viscous forces as against buoyancy forces. Such a conclusion is reasonable for conditions of low stability, but does not seem to be a likely expectation for conditions of high stability. The original formulation of the Richardson criterion involved the assumption that work against buoyancy forces was the principal dissipative mechanism. Thus, some attention is being given to examination of observations in both the boundary layer and in the free atmosphere to try to gain additional insight into the problem of thermospheric turbulence. As indicated in earlier reports, this bears directly on the question of the effectiveness of turbulence as a mechanism for removal of heat from the thermosphere.

OGO 6 measurements of atomic oxygen have shown a minimum over the equator when compared to higher latitudes. Since the atomic oxygen supply over the winter hemisphere is largely supplied by horizontal transport from the summer hemisphere, a minimum over the equator presents a real

problem--how less dense concentrations over the equator can be increased as atomic oxygen is transported into the winter hemisphere. A possible explanation is that motions on the average are not horizontal, but slightly sloping downward away from the equator or upward toward the equator. Such a situation exists in the stratosphere where poleward motions generally include a downward component and equatorward motions an upward component. Thus air at 15 km over the polar regions tends to mix quasi-horizontally with air at about 23 km over the equator. Air moving from the equator toward the poles undergoes a compression associated with its downward motion. A spectacular result of this is the production of higher ozone concentrations over the winter polar region (where no ozone is formed in place because of the lack of sunlight) than in the source region near the equator. If motions in the lower thermosphere have similar slant-wise properties, it would be possible to produce higher atomic oxygen concentrations in the winter hemisphere than over the equator, even though the atomic oxygen in the winter hemisphere is supplied largely by transport across the equator. It would also be possible to produce the minimum over the equator by this means as summer hemisphere concentrations would be reduced as air approaches the equator from the summer hemisphere.

There seems to be no easily stated physical reason why the motions in the stratosphere have the slant-wise properties mentioned above. However, the empirical evidence is clear, and the motions are also produced by the general circulation models of the atmosphere. The isentropic surfaces have a similar, but lesser slope, and the difference in slopes

produces a poleward transport of heat, as would be expected from the distribution of heat input. (If no heat were added or subtracted by radiation, the potential temperature would be conserved and the surfaces of constant potential temperature would have the same slope as the quasi-horizontal mixing motions. With poleward heat transport, the slopes of the constant potential temperature surfaces are less than those of the quasi-horizontal motions; the slopes of the constant potential temperature surfaces would be larger than the slopes of the average motions for equatorward transport of heat.) The behavior of the stratosphere is not necessarily a good indicator of what to expect in the way of behavior of the lower thermosphere but it may well suggest concepts that are worthy of further exploration.

Planetary Mass Spectrometers

W. B. Hanson and J. H. Hoffman

The design of a novel instrument, an energy analyzing mass spectrometer, was described in some detail here in the last report. This satellite instrument utilizes the ram energy of the ambient neutral gases to distinguish them from surface effluents, whether these be indigenous to the walls or atmospheric particles that have impacted the instrument surfaces. This selection feature is necessary for the unambiguous detection of the important atmospheric constituents O_2, N, and NO, whose concentrations have not been determined by conventional closed source mass-spectrometers.

The device is also planned as a dual instrument which will determine both ambient neutral and ambient ion concentrations. In addition, it is planned to be able to measure the energy distribution of the ambient neutral gases in the satellite frame of reference. From these energy spectra it is hoped that the ram component of neutral wind and perhaps even the neutral gas temperature can be determined. Both of these objectives must be regarded as speculative at this time.

A flight opportunity for this instrument, called EAST (Energy Analyzing Spectrometer Test), will take place on Atmosphere Explorer E which is to be launched into a near equatorial (20.1^{o} inclination) in late 1975. The hardware has been built with funds from this grant and the instrument has been delivered to RCA for incorporation into the payload. The instrument was designed to fit the mechanical footprint and electrical interface of the Magnetic Ion Mass Spectrometer (MIMS) which is on Atmosphere Explorers C and D, but not on AE-E, so that there is minimal impact on the project.

At present there is a request by the AE-team to put data from the test device into the United Abstract data files of the Sigma 9 computer in the same file words that the MIMS instrument is alloted on AE-C and D. This may prove awkward, however, because the data itself will not be analyzed on the Sigma 9, but will be decommutated and sent to Dallas for analysis. This poses no real problem for the neutral atmosphere data, except how to insert the results back into the Sigma 9 in a timely manner. A more serious difficulty arises with the ion data, which is a necessary

adjunct for the optimum analysis of the RPA data on AE. An intolerable delay in the RPA analysis may result from the presently planned logistics.

Substantial effort will be expended during 1975 on the development of software to analyze the data from EAST. Because of the many novel features of the instrument, and the built in options to carry out a variety of tests, the required software is rather extensive.

We have proposed that a "next generation" EAST be included in the Electrodynamic Explorer payload, but at the time of this writing the EE instrument selection has not been announced.

Theoretical Study of Ionized and Neutral Hydrogen and Helium in Planetary Atmospheres

E. L. Breig

Of the principal constituents of planetary atmospheres, perhaps least is known about the quantity and variability of neutral atomic hydrogen, primarily because of the lack of good in-situ mass spectrometric data. Hence, even for the terrestrial atmosphere, the bulk of information has emerged from remote optical observations.

Ionospheric measurements, with the proper instrumentation, are also capable of yielding information on neutral hydrogen concentrations over a restricted altitude range. For regions of the terrestrial thermosphere below about 350 km, rates for the charge-exchange reaction, $H + O^+ \rightleftarrows H^+ + O$, are sufficiently greater than the diffusion rates that the concentrations

of H^+ in these regions are determined completely from this reaction. Under such conditions, the neutral hydrogen concentrations [H] must satisfy the relationship:

$$[H] = K\,[H^+]\,[O] \,/\, [O^+]$$

where the equilibrium constant K increases slightly with temperature in the F region.

The above technique has been utilized to derive neutral hydrogen concentrations for the terrestrial thermosphere from concurrent in-situ measurements of H^+, O^+ and O with instruments onboard the AE-C spacecraft. The most critical measurements are those of the small concentrations of H^+; such data are available from AE-C to altitudes well below 200 km. Studies to date have emphasized data spanning several weeks of low magnetic activity in early February, 1974. The results to be discussed thus refer to the early afternoon at the middle latitudes in the winter hemisphere.

The figure provides a plot of the hydrogen concentrations for two superimposed orbits. These data are representative of those analyzed for the above period. The concentrations are ordered in terms of altitude, although in reality they refer to measurements performed along the satellite track and hence involve possible horizontal variations. This deficiency, inherent in most satellite data, is further discussed later in the report. There are two noteworthy features of the data presented in the figure:

(a) The first is the magnitude of [H] between 250 and 300 km. The present data suggest [H] $\sim 3 \times 10^5$ atoms/cm^3 for the winter daytime exosphere at solar minimum ($T_\infty \sim 900°K$), but this level is influenced strongly by the exospheric temperature and by various exospheric loss and redistribution processes.

(b) The second characteristic of the [H] profiles is the low-altitude concentration gradient which is dependent upon the neutral temperature gradient, the diffusion coefficient, and the vertical flow rate of neutral atomic hydrogen.

Preliminary analysis of the data has been in terms of a one-dimensional steady-state model. In such a formulation, the variation of [H] with altitude z, is described by the following equation:

$$\frac{d}{dz}(\ln [H]) = -\left\{\frac{1}{H^*} + (1+\alpha)\frac{d}{dz}(\ln T)\right\} - \frac{S}{[H]}$$

where H^* represents the scale height for atomic hydrogen at temperature T, and α is the coefficient for thermal diffusion. The parameter S is defined in terms of the vertical flux ϕ and the molecular diffusion coefficient D:

$$S = \phi/D$$

The observed hydrogen concentration was inserted as boundary condition at 300 km; the above differential equation was numerically integrated downward in altitude, using the analytic form of the neutral temperature profile given by Jacchia (1971).

Tests have been made of the effects of possible variations in the exospheric temperature and the neutral temperature gradient, however

the flow term S appears to be the most significant parameter. Considerable uncertainty exists in the literature with regard to the magnitude of the diffusion coefficient D, hence the present analysis is unable to establish a unique value for the vertical flux ϕ. If one adopts as reference the theoretical expressions for D as given by Kockarts and Nicolet, a hydrogen upward flux of the order of 2-3 x 10^8 atoms /cm^2/sec is required to fit the low altitude portions of the [H] profiles in the figure. Such a vertical flux is several times larger than that which might be attributed to a Jeans-type escape rate; hence either the diffusion coefficients used are too large or else other mechanisms appear to control the escape of hydrogen from the exosphere.

The above results must be considered as preliminary, with further study required in several important areas. A basic need continues to be better estimates for the molecular diffusion of neutral atomic hydrogen through the principal thermospheric gases. Additional data is also required on possible horizontal variations of [H], in particular a latitudinal or seasonal effect. The special phase of the AE-C mission where the orbit is circular between 275 and 350 km should prove invaluable in this respect. First-looks at several orbits of such data suggest a winter relative enhancement of exospheric hydrogen; extrapolated to lower altitudes this effect would serve to decrease the concentration gradients at the lower altitudes in the figure. The resultant effects on the derived vertical flux are thought to be minor, but such a conclusion requires detailed confirmation. In any case, the results described above are considered to be the first direct experimental determination of the daytime vertical hydrogen fluxes outside the polar region.

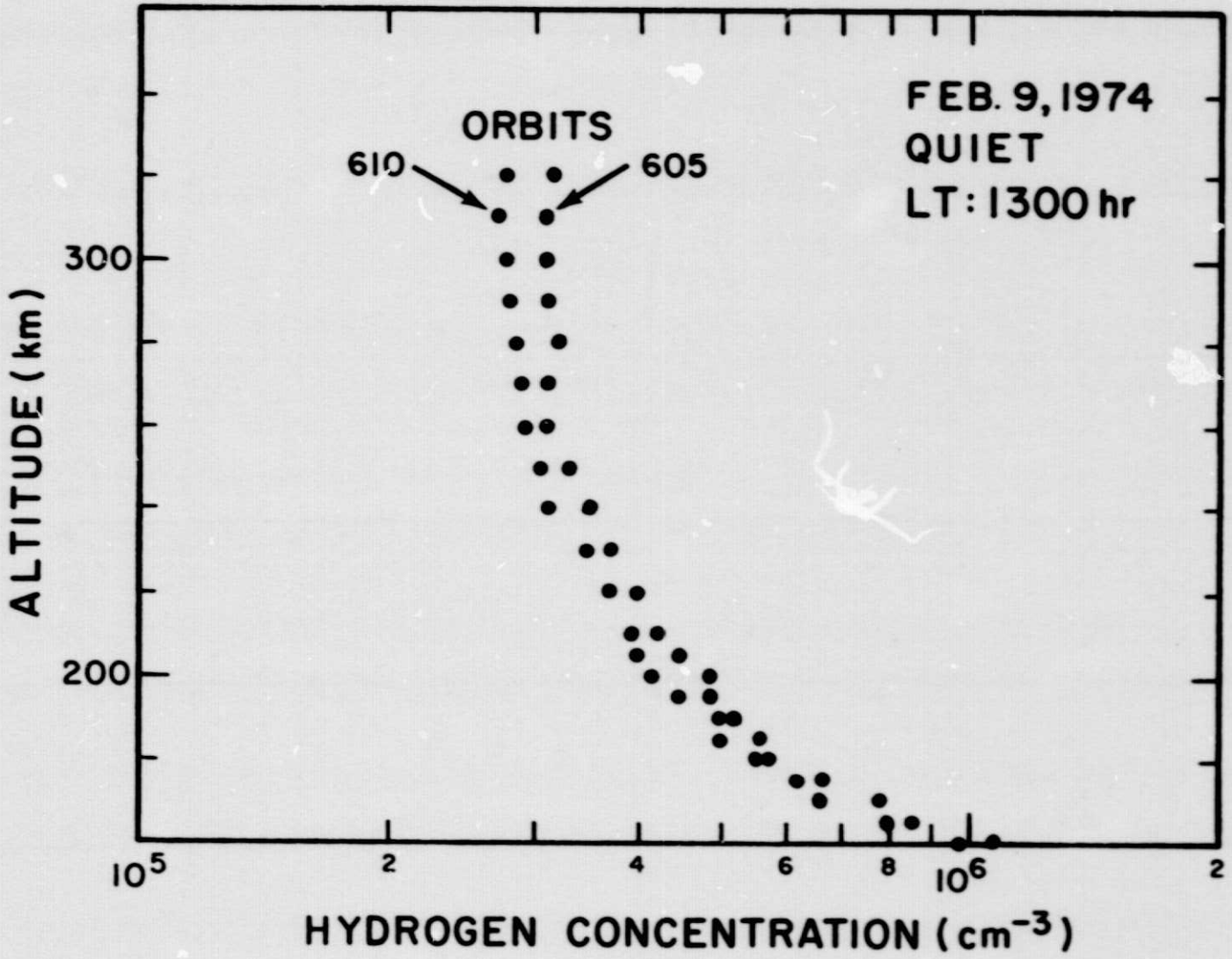
FEB. 9, 1974
QUIET
LT: 1300 hr
ORBITS
610
605
300
200
ALTITUDE (km)
10^5
2
4
6
8
10^6
2
HYDROGEN CONCENTRATION (cm^{-3})

E-F Region Coupling and Its Effect in F-Region Neutral Winds

R. A. Heelis

The effect of electrical coupling of the E and F regions on the F region neutral winds and electric fields is being investigated. The small field aligned currents generated in the F-region by the very small relative motion of the ions and electrons perpendicular to the magnetic field can greatly affect the distribution of electric potential in the E-region. The effects are largely controlled by the local time variation of the E-region conductivity, being largest during the nighttime when the conductivity is small.

The E-region conductivities have been calculated first using an ion concentration profile derived from smoothly fitting Chapman functions in the E and F regions. Local time variations in N_mF_2 and N_mE have been taken from ground based ionosonde measurements. It has been demonstrated that the nighttime E-region ion concentration is a critical factor in determining the effect of the electrical coupling of the E and F regions.

The main features of the vertical ion drift observed at the magnetic equator can be reproduced quite well by this simple model but it is clear that a better model of the E-region ion concentration and continuity of the E and F region neutral winds at their interface are necessary to reproduce the observed ion and neutral meridional velocities in both amplitude and diurnal phase. With this intention, nighttime E region ion concentration profiles from the Arecibo Observatory are being combined

with F-region altitude profiles from Atmosphere Explorer in order to establish a more realistic conductivity model in local time and latitude.

Neutral E-region winds with different tidal modes are being investigated in order to establish the continuity between them and the ones derived at higher altitudes from currently available thermospheric models.

The effect of the E-F region coupling is most dramatic at low latitudes in the F region since the field aligned current densities (order 10^{-7} A m^{-2}) are largest there. The proposed model is adequate to investigate these effects, which are also clearly visible in the ground based incoherent scatter observations made at Jicamarca. Suitable changes to the model will be required to extend the boundary conditions to higher latitudes if the data show these coupling effects to be significant there.

Variations in Thermospheric Concentrations

H. C. Carlson

A program of study has been pursued, using a variety of techniques, seeking a better model for and understanding of thermospheric particle concentrations and their variations.

The neutral concentration, composition, and scale height profile near 100 to 120 km exert a profound control over thermospheric behavior, yet reliable data from this region are sparse. Incoherent scatter data on neutral concentrations (extracted from ion-neutral collision frequencies) and temperature data have been gathered at Arecibo in this altitude range. The time continuity of these measurements throughout daylight hours allows

sorting out large amplitude tidal variations from daily mean profiles. These data have been extensively tested for reliability and self consistency. Above 120 km in the lower thermosphere, the temperature gradient at each altitude should very nearly give the net thermospheric heat input above that altitude. Analyses of these temperature gradients indicate roughly a half erg $cm^{-2} sec^{-1}$ down through the 120 km level, consistent with expectations, but give seasonal variations inconsistent with a purely solar EUV heat input interpretation. In winter as compared with the autumnal equinox, significantly lower "mesospheric" (100 km) temperatures and neutral concentrations are found.

Simultaneous 5577 Å airglow observations have also been made at night (at Arecibo with L. L. Cogger) with a similar backscatter program on E and F region and a Fabry Perot for doppler temperatures and a photometer for 5577 Å and 6300 Å intensities. F region recombination calculations fitted to observed electron concentrations and 6300 Å intensities allowed extraction of the 5577 Å F region airglow component to leave the E region residual which results from the three body recombination of atomic oxygen. Variations in this intensity have been interpreted in the literature as variations in n(O), the atomic oxygen concentration. The nighttime E region spectral measurements are normally of little use for purposes of extracting neutral temperatures and concentrations due to poorer signal to noise ratios than by daytime and due to metallic ion concentration uncertainties. However, here the neutral temperature at the appropriate altitude was taken from the Fabry Perot 5577 Å E region temperature, and used in the analysis of the incoherent scatter spectra

(removing one of the interdependent parameters that must normally be solved for in extracting a neutral concentration from the spectra). On one such night, a variation of a factor of about 1.6 in n(O) with a time scale consistent with a tidal mode, was deduced from the 5577 Å intensity variation.

Incoherent scatter data (with Fabry Perot temperature) gave the same factor of variation in total neutral concentration, assuming no significant ion concentration variations, supporting the technique of extracting n(O) concentration variations from E region 5577 Å variations.

Satellite drag models that reasonably represent the mean behavior of F region atomic oxygen concentrations (the dominant constituent in the F region) have existed for some time. However, coincident measurement of the exospheric temperature and atomic oxygen concentration, and measurement of detailed temporal variations of these parameters within the day and from day to day, are in limited supply. Software to extract this information from incoherent scatter data, on the basis of ion heat balance relations, has been put in working order at UTD. Analysis of a limited number of days' data has already confirmed that, as over France, the F region atomic oxygen concentrations over Arecibo (L = 1.5) fall more rapidly at sunset than suggested by satellite drag models. This is not simply a consequence of a more rapidly falling exospheric temperature. Day to day variations have also been found to exist that must be interpreted as significant departures in "base level" n(O) values, and/or low

altitude temperature shapes, relative to those assumed in current Jacchia and CIRA models. An important extention of this work is to apply the technique to high latitudes where less well modeled but dramatic energy sources may introduce important modulations on patterns of neutral concentration variations and circulation. Preliminary analysis (with VB Wickwar) of Chatanika backscatter (L = 5.6) data, in terms of n(O) and neutral magnetic meridional wind patterns, has already strongly suggested some such manifestations. Future emphasis will likely shift toward global variations, including results from more than one incoherent scatter station, and tied together within the context of data gathered with the AE satellite.

A non-trivial "systematic" uncertainty that exists in the incoherent scatter technique, as applied by various groups to date to the extraction of T_{ex} and $n(O)_F$ parameters, should be noted: uncertainty in the heat transfer rate from atomic oxygen ions to oxygen atoms. This rate depends on a resonant charge exchange process and n(O) is inversely proportional to its assumed value. Definition of this charge exchange cross-section is of more general interest and an improved definition of its magnitude will be obtained using a statistical analysis of a large body of data. Normalization will also be provided by satellite drag data and by comparison with individual in-situ coincident measurements by satellite-incoherent scatter overflights (particularly the AE satellite). Data for both of these is now in hand, and under analysis. Preliminary analysis indicates that the value currently used in the literature is some tens of percent high.

Analysis of Incoherent Scatter Data Obtained at the Jicamarca Radar Observatory

J. P. McClure

Major progress has been made in our efforts to process a large body of incoherent scatter data obtained at the Jicamarca Radar Observatory near the geomagnetic equator at Lima, Peru. The data cover the years 1965-1975, and mainly consist of ionospheric Faraday rotation and correlation function measurements, from which the electron density N_e, the plasma temperatures T_e and T_i, and the ionic composition may be inferred.

A data processing routine first developed at The University of Texas at Dallas has successfully been adapted for production use on the CDC 7600 computer at NCAR in Boulder, Colorado. Completely automatic least-squares curve fitting is now being done between the theoretical and measured autocorrelation functions.

Preliminary processing has been completed for the first half of the data (1965-1969). The results consist of compact microfilm plots, which have been designed with the needs of the World Data Center in mind, of the measured and fitted theoretical autocorrelation functions (two frames per radar integration) and the altitude profiles of N_e, T_e and T_i with their respective statistical error bars (one frame per integration). These geophysical results are also recorded on magnetic tape.

At present the processed data is being checked for systematic errors and the processing algorithms are being modified in preparation for a final pass through the data. The second half of the data set (1969-1975) is being shipped from Peru via diplomatic pouch. Approximately 40% of this data set, randomly chosen in time, has reached the United States; when the entire set has been received it will also be processed.

Ion Temperatures in Planetary Ionospheres

E. L. Breig

The magnitudes and variabilities of the charged particle temperatures are important parameters in specifying the states of planetary atmospheres. The temperatures of the positive ions, in particular, describe a special link in the energy transfer process, intermediate between ionizing absorptions of solar radiation and collisional neutral heating, for the undisturbed non-polar regions. Previous reports have discussed the results of studies which pertain to ion temperatures in the winter night-time terrestrial ionosphere, based on data from the retarding potential analyzer onboard the OGO-6 satellite. A rough draft of a manuscript, by E. L. Breig and others, has been completed; copies of the resultant formal document are to be forwarded when available. The following summary has been extracted from said manuscript:

"Ion temperature data have been presented from the retarding potential analyzer on OGO-6. These data refer to the winter mid-latitude nighttime ionosphere between 400 and 900 km, for local time intervals characteristic of both midnight-predawn and post sunset. The adopted mode of analysis provides a decoupling of altitude and horizontal variations; the corresponding results confirm other indications of a well-defined longitudinal dependence for the observed ion temperatures during both local time periods.

An extended longitude region of enhanced ion temperature is particularly evident in the midnight-predawn data, with the greatest longitudinal variation of temperature observed between 600 and 800 km. This

longitude r gion is relatively broad at 50° magnetic dip latitude; however at 30° the temperature data indicate greater structure over a much narrower longitude range. Similar analyses with the concentrations of the major ion, O^+, reveal a consistent increase of plasma scale height within the high-temperature regions. The same general type of longitudinal variability of ion temperature is discernible, but is not as pronounced, in data for the post-sunset period.

Special considerations were given to seasonal and local time changes and to variations in solar and geomagnetic activity during the period of data acquisition. Such effects were, however, concluded to be of secondary importance relative to the resultant interpretation of the data. The appearance and variability of energetic electrons, also observed in the midnight-predawn winter ionosphere, exhibit excellent correlation with changes of solar conditions at magnetically-conjugate latitudes in the southern summer hemisphere. The presence of these energetic electrons in the same general longitude sector as the ion temperature enhancement establishes such particles as a firm candidate for the associated night-time energy source at these longitudes."

Space Science Computation Assistance

J. E. Midgley

The level of usage continues to increase on the PDP 11-45 procured in July 1972, primarily to handle space-related data processing. We now have operators on duty from 6:00 a.m. until 11:00 p.m. to process the jobs submitted. The period from 11:00 p.m. until 3:00 a.m. is regularly

used for development work on the new operating system which is nearly finished and now in the debugging states; and long jobs are frequently run unattended in the 3:00 a.m. to 6:00 a.m. time slot. Thus the computer is nominally in use 24 hours a day now, although the load has not yet (fortunately) increased to the point where it is continually busy during that time. As a result, turnaround is still very good for users with relatively short jobs, and it is hoped that the new system will be operational to increase throughput before the system becomes saturated.

The largest single user is still Dr. J. D. Winningham, who is using it to make microfilm plots of Dr. W. J. Heikkila's ISIS data. Each eight minutes of data is plotted in a single frame which gives an overview to select interesting events and times. Selected times are then plotted and printed out in detail by other programs. The volume of data backlogged and currently generated could absorb all the time available, but the amount of time actually used has in practice been limited to about 6 hours a day on the average, due to excessive down time on the plotter, competition for plotter time from the IBM 360-155 which also uses it, and competition from other users of the 11-45.

Several users average about 2 hours per day each: J. P. McClure, H. C. Carlson, L. Maher, and R. Chaney. Dr. McClure uses it to process radar data on ionospheric irregularities obtained at the Jicamarca Radar Observatory near Lima, Peru. His programs make microfilm plots of the radar data in several different formats, including an intensity-modulated format using the full dynamic range of intensities available on the plotter. Dr. Carlson is using it to reduce a large body of incoherent scatter observational data to obtain charged particle temperatures and

concentrations in the earth's thermosphere. These are being further processed to deduce upper atmospheric neutral temperatures and concentrations. Some atmospheric model calculations are also being performed. Some calculations are also being made relating to ionospheric photoelectron fluxes and their "wave-particle" interactions. Louis Maher, a student of Dr. B. A. Tinsley, is using it to develop models for the ionosphere and neutral atmosphere using AE data at one altitude and the diffusion equations. He plans to use this as the basis for H escape calculations. Dr. Chaney is just completing a theoretical study of color centers in LiF, and his student, Uma Seth, is calculating the energy band structure of CaO.

Dozens of other users regularly use it for an hour or less each day. For example, Dr. F. R. Allum recently finished copying and reformatting 290 tapes of Explorer 34 and 41 data from 7 track to 9 track so that they could be processed more efficiently on the IBM computer. R. A. Spiro is plotting Dr. W. B. Hanson's AE-C drift meter data, and using it to deduce polar convection patterns. An interface has been established between the 11-45 and the Sanders terminal to the AE Sigma 7 at Goddard Space Flight Center. Some special software makes it possible to collect data at a slow rate from the terminal simultaneous with the execution of other programs. This data is then dumped to tape for later plotting. The link is currently being used to transfer Ion Composition and Drift Meter data from AE-C.

OGO 6 Ion Concentration and Ion Irregularity Data

W. B. Hanson

The Retarding Potential Analyzer Data from OGO 6 constitute the only proven reservoir of satellite ion temperature data prior to Atmosphere Explorer. Similarly, the most sensitive and comprehensive body of data on ionospheric irregularities is available from the same instrument. Because of the unique nature and excellent quality of these results it is important to have the data reduced to useful forms and to have it generally available.

The data analysis and presentations have been refined over a period of years and the data bank has now been completely processed, insofar as this seems fiscally responsible. All of the data output has now been summarized on 30 magnetic tapes and several rolls of microfilm in different formats. These are now in the process of being sent to the NASA World Data Center. With the completion of this effort we can now examine the large body of data in an orderly manner for morphological characteristics, as well as make comparisons with data from other OGO 6 measurements.

A rather elaborate data key has been written to supplement the magnetic tape and film that are being shipped to the World Data Center. The description of the tapes fills a volume that is too large to append here, but the summary page for the tapes and a description of the data included are attached. The film description is more modest and has been appended in its entirety.

OGO VI RPA DATA

OGO VI was launched on June 5, 1969 into an 82^{o} inclination prograde orbit, with nominal apogee and perigee of 1100 km and 400 km. The initial orbit plane was in a near dawn-dusk configuration, and it rotated approximately two degrees local time each day. After nearly two weeks of normal operation a malfunction in the solar power system caused the vehicle potential, ψ_s, to have a large negative value ($|\psi_s| > 20$ volts) when the spacecraft was sunlit. Subsequently, the daytime magnitude of ψ_s changed discontinuously on several occasions, and during late 1969 and early 1970 it did not exceed 14 volts. Gradually the vehicle system lost capability and it became increasingly unreliable to read out the tape recorders. The spacecraft was finally turned off as a fiscal expediency in late 1971, with several of its instruments, including the Retarding Potential Analyzer, still in perfect working order.

OGO VI proved to be an excellent scientific spacecraft. It provided in excess of 5000 complete orbits of data during its lifetime. The principle devices that supplied aeronomical data were the RPA, a neutral mass spectrometer, a Bennett ion mass spectrometer, a single axis electric field experiment, 6300 A and 5577 A airglow photometers, and a 6300 A interferometer for measuring the neutral atmospheric temperature. Some langmuir probe data are also available, as are some energetic particle data ($E > 20$ Kev), and some electromagnetic wave intensity data over wide frequency ranges. Very limited syntheses of data from the various instruments have been carried out to date.

The RPA data that is available in the World Data Center comprises nearly all the data that could be analyzed for ion temperature. In addition, much more data is included that provides an irregularity index for the total ion concentration, N_i, as well as a parameter that closely characterizes N_i itself. During the first 240 orbits when ψ_s was well behaved the ion temperature was measured over the complete orbits. After ψ_s became large in sunlight the Retarding Potential could no longer repell ions from the collector and current voltage characteristic curves could not be obtained except when the spacecraft was in eclipse. During a four month period at the end of 1969 and the beginning of 1970 $|\psi_s|$ decreased to below 14 volts and it was possible to analyze the sunlit data for T_i, and for H^+, He^+, and O^+ ion concentrations. We call this "good-bad" data; it is of variable quality, but always less reliable than the sunlit data from orbit numbers less than 240. Not all of the "good-bad" daytime data was analyzed.

The RPA data appears in three different plot forms, only two of which exist for all the data analyzed, and only these two are available from the World Data Center. All of the data in these two summary film plots, called SAT plots and Sigma plots, are also available on a set of 30 800 bpi magnetic tapes. The other plot format, called OGO plots, is a plot of the individual ion characteristic curves and the essentially raw irregularity data. This primary data plot format was essential for developing confidence in the data analysis techniques employed and for resolving questions that arise from peculiar behavior observed in the summary data plots. Many such questions continue to arise as we examine new summary data, but unfortunately OGO plots do not exist for most of the data because of economic considerations.

Any prospective user of the RPA data would be well advised to examine at least one roll of OGO plot film in order to obtain a feel for the raw data, and for the curve fitting that provides most of the summary plot numbers.

OGO 6 RPA BIBLIOGRAPHY

"Plasma Measurements with the Retarding Potential Analyser on OGO VI," with S. Sanatani, D. Zuccaro, and T. W. Flowerday, J. Geophys. Res., 75 (28), 5483, 1970

"Meteoric Ions above the F_2 Peak," with S. Sanatani, J. Geophys. Res., 75 (28), 5503, 1970

"The Relationship between Fe^+ Ions and Equatorial Spread F," with S. Sanatani, J. Geophys. Res. 76, 7761, 1971

"Errors in Retarding Potential Analyzers Caused by Nonuniformity of the Grid Plane Potential," with D. R. Frame and J. E. Midgley, J. Geophys. Res. 77, 1914, 1972

"Molecular Ions in the F2 Layer," with H. Rishbeth and P. Bauer, Planet. Space Sci. 20, 1287, 1972

"Satellite and Ground Based Observations of a Red Arc," with A. F. Nagy, T. L. Aggson and R. J. Hoch, J. Geophys. Res. 77, 3613, 1972

"The Source and Identification of Heavy Ions in the Equatorial F Layer," with D. L. Sterling and R. F. Woodman, J. Geophys. Res. 77, 5530, 1972

"Comparison of T_e and T_i from OGO 6 and from Various Incoherent Scatter Radars," with J. P. McClure, A. F. Nagy, R. J. Cicerone, L. H. Brace, M. Baron, P. Bauer, H. C. Carlson, J. V. Evans, G. N. Taylor, and R. F. Woodman, J. Geophys. Res. 78, 197, 1973

"OGO-6 Measurements of Supercooled Plasma in the Equatorial Exosphere," with A. F. Nagy and R. J. Moffett, J. Geophys. Res. 78, 751, 1973

"Large N_i Gradients Below the Equatorial F Peak," with S. Sanatani, J. Geophys. Res. 78, 1157, 1973

"On the Cause of Equatorial Spread F," with J. P. McClure and D. L. Sterling, J. Geophys. Res. 78, 2353, 1973

"Effects of Interhemisphere Transport on Plasma Temperatures at Low Latitudes," with G. J. Bailey, R. J. Moffett and S. Sanatani, J. Geophys. Res. 78, 5597, 1973

"A Catalog of Ionospheric F Region Irregularity Behavior Based on Ogo 6 Retarding Potential Analyzer Data," with J. P. McClure, J. Geophys. Res. 78, 7431, 1973

"In Situ Measurements of the Spectral Characteristics of F Region Ionospheric Irregularities," with P. L. Dyson and J. P. McClure, J. Geophys. Res. 79, 1497, 1974

SUMMARY OF MAGNETIC TAPE INFORMATION

OGO-6 F-03 Retarding Potential Analyzer

Dr. W. B. Hanson
The University of Texas at Dallas

Tape Number	Started				Stopped			
	Orbit	Year	Day	Time	Orbit	Year	Day	Time
WDB001	20	1969	158	2825	814	1969	213	796
WDB002	815	1969	213	1635	1031	1969	227	83279
WDB003	1032	1969	228	3594	1242	1969	242	53655
WDB004	1243	1969	242	53665	1839	1969	283	78824
WDB005	1840	1969	283	78833	1979	1969	293	51020
WDB006	1980	1969	293	51029	2115	1969	302	85521
WDB007	2116	1969	302	85531	2259	1969	312	81220
WDB008	2260	1969	312	81229	2423	1969	324	23373
WDB009	2424	1969	324	23382	2582	1969	335	21940
WDB010	2583	1969	335	21950	2727	1969	345	23198
WDB011	2728	1969	345	23208	2878	1969	355	60171
WDB012	2879	1969	355	60180	3013	1969	365	1594
WDB013	3014	1969	365	1603	3183	1970	011	65349
WDB014	3184	1970	011	65359	3358	1970	023	72426
WDB015	3359	1970	023	72435	3542	1970	036	46585
WDB016	3543	1970	036	46595	3770	1970	052	23616
WDB017	3771	1970	052	23625	3989	1970	067	32886
WDB018	3990	1970	067	32895	4334	1970	091	14919
WDB019	4335	1970	091	14929	4549	1970	105	86114
WDB020	4550	1970	105	86124	4739	1970	119	4014
WDB021	4740	1970	119	9200	4905	1970	130	46005
WDB022	4906	1970	130	46015	5114	1970	144	79678
WDB023	5115	1970	144	82060	5803	1970	192	31179
WDB024	5804	1970	192	31189	5989	1970	205	13591
WDB025	5990	1970	205	13600	6176	1970	218	1691
WDB026	6177	1970	218	1700	6476	1970	238	56263
WDB027	7020	1970	276	392	7738	1970	325	31024
WDB028	7739	1970	325	33644	8719	1971	027	59359
WDB029	8720	1971	027	59368	9978	1971	113	80041
WDB030	INDEX							

In the latter case the plotted values are nearly proportional to the Fe^+ concentration. We cannot simultaneously determine both an electron flux and the Fe^+ concentration. Usually this is no problem since Fe^+ is confined to dip latitudes $< \pm 30°$ and conjugate photo electrons and auroral electrons generally occur at higher latitudes. In the daytime, photoelectrons mask the presence of Fe^+.

The magnitude of the electron flux is obtained by dividing the negative current to the collector by the effective area of the aperture (i.e., including grid transmission). The flux is then 2.9×10^6 cm^{-2} sec^{-1} per bit (1 bit = 6×10^{-13} amps). A full geometrical calculation shows that for an isotropic maxwellian photoelectron gas with a temperature of 7 ev, the ambient flux above 10 ev (+ spacecraft potential) is approximately 10^6 electrons/cm^2 sec ster bit.

The zero level of the electrometer drifts between the zero and 3 bit levels though the noise level is small compared to one bit. Most of the data plotted has been corrected for this effect, except when Fe^+ is present. Unfortunately, some of the plots erroneously show the zero level plotted as an electron flux.

The derivation of the various ion concentrations assumes that the plasma is at rest in the earth's frame of reference, and that the molecular ions have a mass of 30 AMU. Often this leads to an incorrect ratio of (H^+/He^+) ions near the equator when the inter-hemisphere plasma velocity is large. This same plasma motion causes the derived values of T_i to be too large or too small, depending on

whether the plasma motion is toward or away from the satellite, respectively.

The statistical errors in T_i are normally quite small when $n(O^+) > 10^3$ cm^{-3}, but if the Stanford antenna on the spacecraft is being positively biased in pulses a periodic structure in T_i can be observed, whose amplitude is rather larger than the error bars. These are not real changes in T_i induced by the transmitter, but faulty ion curves distorted by the antenna pulses. This condition can only be confirmed by examining the OGO plots. Orbit numbers 3029 to 8330 were flown in 1970; smaller orbit numbers refer to 1969 and larger numbers to 1971. New orbits are commenced when the satellite traverses the equatorial plane from South to North.

On some orbits the OPEP (orbital plane experimental package) on which the RPA is mounted is scanned continuously through ram and into the wake and back again. The data from these orbits is not very useful, but is easily recognized by the periodic disappearance of the plasma. The values taken near the ram have some validity if taken in the fast mode.

Definition of Parameters

ALT - satellite altitude in km

LNG - geographic longitude

LAT - geographic latitude

LT - local time in hours and minutes

DIP - magnetic dip angle in degrees

Z - solar zenith angle in degrees

NH - solid earth (solar) screening height at north conjugate point

SH - solid earth (solar) screening height at south conjugate point

L - McIlwain L parameter

SA - angle between normal to sensor face and the sun

UT - universal time in seconds of the day

SAT PLOT

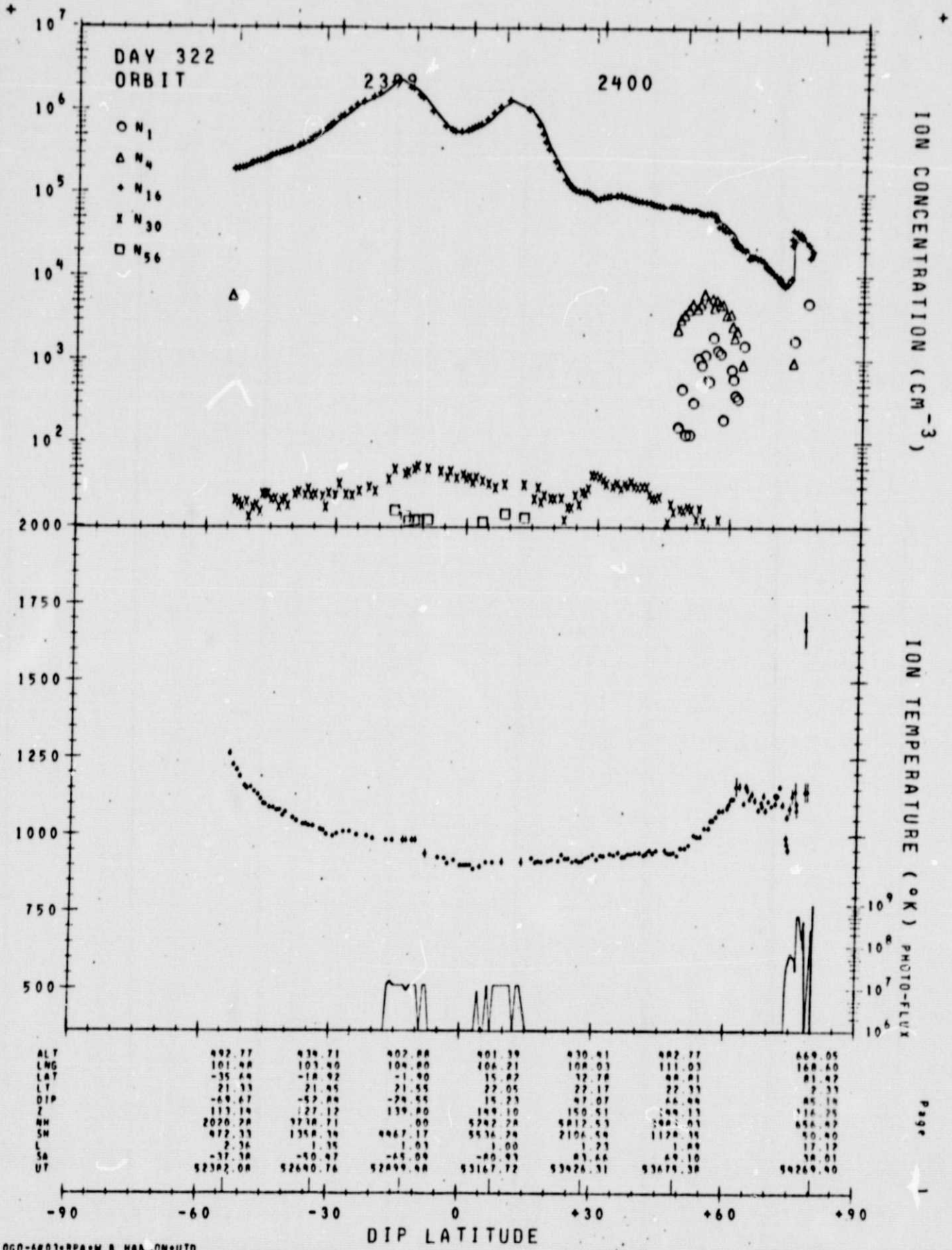

ORIGINAL PAGE IS
OF POOR QUALITY

RPA SIGMA PLOTS

Each frame of SIGMA PLOTS displays up to 60 minutes of reduced Ogo 6 RPA data, starting at middle latitudes ($\Lambda \geq$ 35° or $\leq$ -35°) and crossing the polar cap and the subsequent middle, low and middle latitude regions. The quantities plotted are the total ion (electron) concentration, the ionospheric irregularity index ($\Sigma = \Delta N_i/N_i$, RMS%), the satellite altitude, the altitude of the earth's shadow at the northern and southern end of the satellite's geomagnetic field tube, the size of the ionospheric irregularities (km/peak), and, where available, the ion temperature, the ion concentrations $[16^+]$, $[30^+]$, $[56^+]$ and $[4^+ + 1^+]$, and the photoelectron flux. These latter parameters (temperature, ion composition data and flux) are usually available only during satellite eclipse.

Blocks of orbital parameters are provided at the bottom, and the dip latitudes where these data blocks apply (2 to 10 data blocks are provided) are indicated by the numbers 1 through 10 shown on the lower scale. Parameters provided are invariant latitude, magnetic dipole local time, local time, longitude, latitude, solar zenith angle, sun angle (angle between the sun and the normal to the RPA aperture plane), universal time, and satellite altitude.

The polar plot in the lower left corner gives the value of $\Sigma(\Delta N_i/N_i$, RMS%) versus invariant latitude and dipole local time along the satellite track. The smallest dots indicate $\Sigma < 1\%$; the medium dots, $1\% < \Sigma < 10\%$; and the large dots, $\Sigma > 10\%$. The dots plotted are obtained from the 5-point running means, which are the circles connected by a heavy line on the plot at the top of the frame.

Just below the Σ plot the satellite altitude is indicated by the sinusoidal curve (perigee ~400 km, apogee ~1100 km). The symbols N and S give the altitude of the earth's geometrical shadow, assuming no screening by the earth's atmosphere, at the northern and southern intersection of the earth's surface and the geomagnetic field line through the satellite. The determination of these screening heights, which are significant for anticipating the presence of conjugate photoelectrons, is often faulty, but even the nonsense values have been plotted. Superimposed on the altitude plots is a plot of electron flux (cm^{-2} sec^{-1}) of energy greater than 10 ev, unless Fe^+ is present. In the latter case the plotted values are nearly proportional to the Fe^+ concentration. Because of a 20 volt limit on the retarding potential we cannot simultaneously determine both the electron flux and the Fe^+ concentration, but usually this is no problem because Fe^+ is observed only for dip latitudes $< \pm 30°$ and auroral electrons or conjugate photoelectrons generally occur only at higher latitudes.

The size parameter plotted next is of limited utility because of inadequacies in the algorithm used to calculate it. In particular, the upper limit occurring between 30 and 40 km is set by the distance the satellite travels during the fast "duct" or irregularity-measuring operation,* and has no geophysical significance.

Ion temperatures are plotted as a small dot with a vertical error bar whose length corresponds to the statistical error in T_i. These error bars often lie entirely within the dot. The density of T_i points plotted is variable, depending on the instrument mode, on the quality of the data and on the fraction of data properly interpreted by the analysis algorithms.

*See the OGO Plots write-up

Bad fits* are rejected by an arbitrary criterion: if the RMS deviation between the best-fitting theoretical curve and the experimental points exceeds 10%, the N_i and T_i values derived are not plotted. Occasional values are plotted which are obviously incorrect, usually because of an electrometer ranging error. In these cases N_i will be one or more factors of $\sqrt{10}$ above or below the correct value of N_i.

When the satellite is not in eclipse (and after orbit 240) the total N_i value and the Σ values can still be obtained, even though the (-) satellite potential is usually too large to measure T_i. The derived N_i, however, is somewhat larger than the ambient value, owing to the ion focussing of the very negative spacecraft. The magnitude of this overestimate is larger the greater the proportion of light ions (H^+ and He^+) present. Factors of order 2 are involved. From day 297/69 to day 055/70 it is still possible to deduce daytime T_i values, though with lower accuracy, because the satellite potential is smaller than 14 volts when the satellite is in sunlight during this period.

The total $N_i(N_e)$ value often shows a great deal of randomness when the satellite is not eclipsed because of faulty algorithms used for the determination of this quantity. Very often the eye can follow the actual changes in N_i, despite this weakness, but we apologize for this failure. Whether the satellite is or is not eclipsed, the derivation of the various ion concentrations assumes that the plasma is at rest in the earth's frame of reference, and that the molecular ions have a mass of 30 AMU. Often this leads to an incorrect ratio of (H^+/He^+) ions near the equator when the

*See the OGO Plots write-up

interhemisphere plasma velocity is large. This same plasma motion causes the derived values of both N_i and T_i to be too large or too small, depending on whether the plasma motion is toward or away from the satellite, respectively.

SIGMA PLOT

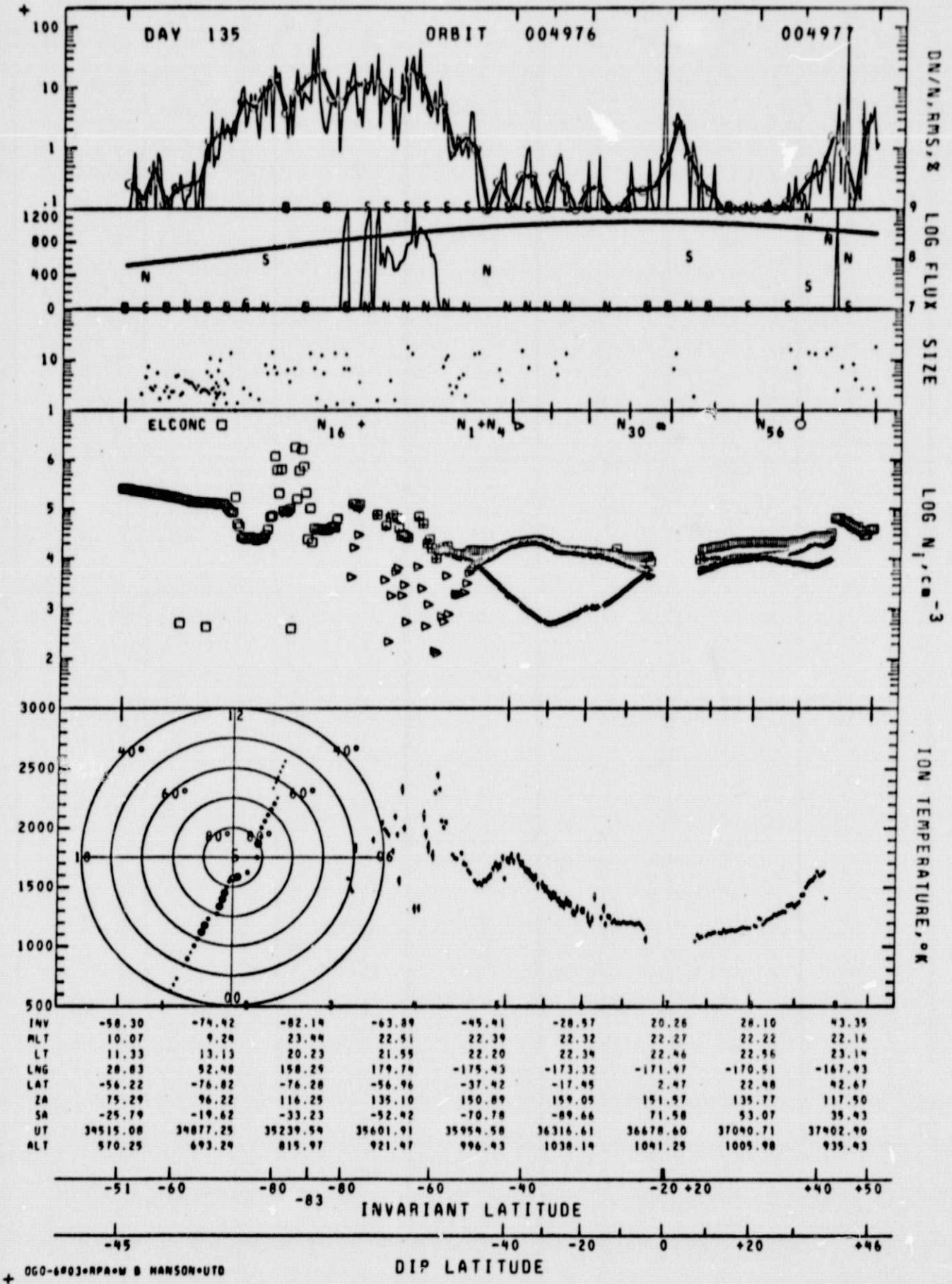

RPA OGO PLOTS

Each frame of this plot shows four separate data sequences, each having one "sweep" and one "duct" operation. The left hand side shows a logarithmic plot of ion current versus retarding potential, where the plotted points are experimental and the line is a theoretical fit to the data (see Hanson et al., 1970, for details). The right side contains the "duct" data and reveals the changes in ion concentration observed along the satellite flight path. Various geophysical coordinates are printed out between the data plots. Data can be recorded in either the fast or slow mode. In the fast mode the ion sweep and the duct operation each take approximately 5 seconds, whereas in the slow mode they are allotted 20 seconds each. So many points are plotted in the slow ion sweeps that one cannot usually see the theoretical curve plotted through them.

The derived values of ion temperature and ion concentrations are printed out in the middle for each sweep that is analyzed, together with their statistical error bars. Also given are the vehicle potential and σ, the mean square fractional deviation of the measured points from the least-squares best-fit theoretical curve. The Julian day number is given, but the year must be inferred from the Orbit number. Orbits 3029 to 8330 were flown in 1970; smaller numbers refer to 1969 and larger orbit numbers to 1971. The quantity called electron flux is derived from the currents observed at large retarding potentials. When the value (cm^{-2} sec^{-1}) is followed by an asterisk it is proportional to the electron flux (greater than ~10 ev) that is observed and the ion currents plotted have been corrected by an appropriate amount. The

absolute magnitude assigned to the flux is somewhat arbitrary and is based on the measured electron current per unit effective aperture area. The numbers are of qualitative value for satellite eclipse data (most of the data) in that they reveal the presence of conjugate photoelectrons when moving toward the magnetic equator and reflected conjugate photoelectrons when moving away from the magnetic equator. An estimate of the absolute electron flux of electrons with energy greater than 10 ev in particles/cm^2 sec ster assuming an isotropic flux can be obtained by dividing the printed number by π, if the "temperature" of these electrons is approximately 7 ev.

In addition, the presence of secondary electron fluxes at high latitudes (usually $>60°$ dip) is commonly observed. This invariably signifies the presence of diffuse aurora in the absence of sunlight or conjugate electrons. The auroral fluxes are usually much more variable than photoelectron fluxes. When the flux value is greater than 9×10^6 cm^{-2} sec^{-1} but not followed by an asterisk this usually signifies the presence of Fe^+ ions (if the dip latitude is less than $\sim 30°$). For most of the data (but not all) the flux number is of the order 10^{-12} and in this case the number refers to a zero correction (in amperes) that has been made to the electrometer data before curve fitting or plotting (6×10^{-13} amps corresponds to a one bit correction; the electrometer noise level is of order 10^{-13} amp.).

The logarithmic ion current values have been obtained from an automatic ranging linear electrometer, and occasionally the deranging algorithm incorrectly adds or deletes a range change (a gain change of $\sqrt{10}$) resulting in an invalid ion characteristic curve. These curves are analyzed along with the rest, though they usually give larger σ values and error bars.

When the electrometer output is sampled while the electrometer is ranging the resulting data can be faulty. The program does not include the first point after a range change in the least squares analysis but does plot them with circles around them. For various reasons the data reduction program sometimes uses the wrong ion masses in the analyses, or incorrectly identifies an ion current region with the wrong ion mass. This results in invalid T_i, ψ, and N_i values. Most of the time these errors are readily recognized and the points are usually not plotted in SAT or SIGMA PLOTS because $\sigma > 10\%$.

There are two signals plotted during the duct period, the electrometer output and the duct amplifier output. The dots give the electrometer output, which is proportional to the total ion flux entering the RPA ($N_i V_s$). The magnitudes of the dot values have been normalized to unity at the beginning of each duct frame and fractions from 0 to 2 are plotted, though occasionally the actual values can exceed twice the initial value. Very large amplitude small scale structure is encountered where the instrument is completely aliased; changes in the electrometer sensitivity probably occur during these times but it is difficult to prove this. The continuous line joins points from the duct amplifier which have 1/3 the separation of the dots; this line shows variations from the initial ion concentration that can vary from +5% to -5%. Depending on the initial electrometer output voltage the duct amplifier may saturate at percentage changes smaller than $\pm 5\%$. This saturated condition is easily recognized.

The numbers (S's and Σ's) written at the top of the duct frames are derived values of irregularity scale size (S) and amplitude (Σ). The scale size S is derived from an algorithm which detects and counts peaks whose amplitude exceeds a certain threshold value above the previous minimum. The S values are given in units of km/peak. The parameters S_{11} and S_{12} are

derived from the amplifier output (continuous line) and refer to peaks >.3% and 1.0%, respectively. The parameters S_{21} and S_{22} are derived from the electrometer output and refer to peaks >3% and 10%, respectively. In practice, the S values have not been very meaningful, or useful.

The Σ values are given in dimensionless units corresponding to the RMS value of $\Delta N_i/N_i(\%)$. The parameters Σ_{11} and Σ_{12} are derived from the amplifier output, and refer to RMS percentage deviations from a horizontal straight line and a straight line joining the first and last points (before saturation), respectively. The parameters Σ_{21} and Σ_{22} are derived from the electrometer output (dots), and as before, refer to the RMS percentage deviations from a horizontal straight line and a straight line joining the first and last points, respectively. These Σ values are very useful in characterizing the relative smoothness (or roughness) of the ionosphere and they constitute the principal parameters of the Sigma plots.

At the top of each duct frame are given the electrometer sensitivity range for the maximum ion current in the previous ion sweep, together with the saturation electrometer voltage on that range at the start of the duct period. These quantities specify the ion current to which the duct electrometer plots have been normalized.

OGO PLOT

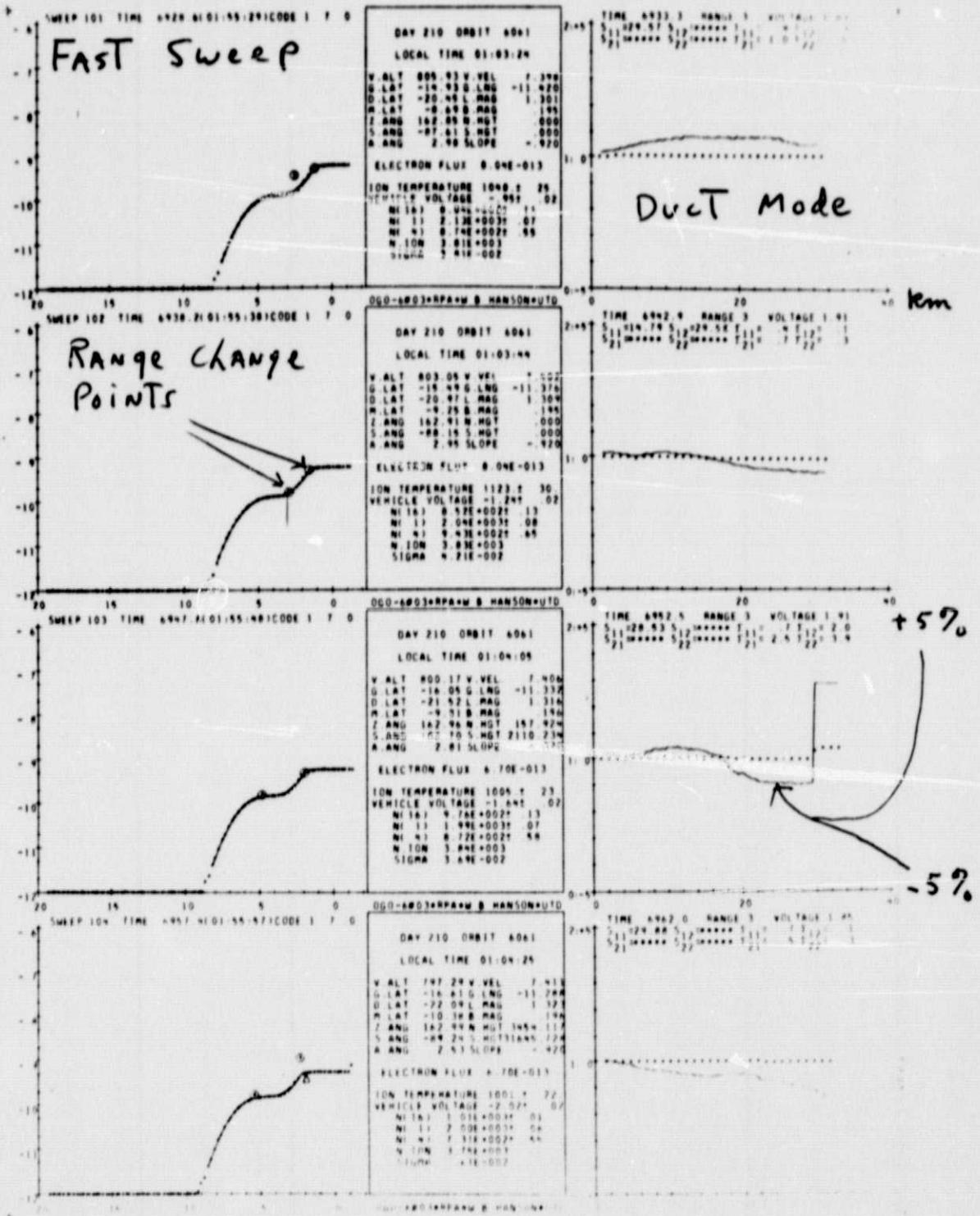

OGO PLOT